

Voids effect on micromechanical response of elastoplastic fiber-reinforced polymer composites using 1D higher-order theories

Original

Voids effect on micromechanical response of elastoplastic fiber-reinforced polymer composites using 1D higher-order theories / Petrolo, M.; Pagani, A.; Trombini, M.; Carrera, E.. - In: MECHANICS OF MATERIALS. - ISSN 0167-6636. - ELETTRONICO. - 184:(2023). [10.1016/j.mechmat.2023.104747]

Availability:

This version is available at: 11583/2980725 since: 2023-07-27T07:28:35Z

Publisher:

Elsevier

Published

DOI:10.1016/j.mechmat.2023.104747

Terms of use:

This article is made available under terms and conditions as specified in the corresponding bibliographic description in the repository

Publisher copyright

(Article begins on next page)



Research paper

Voids effect on micromechanical response of elastoplastic fiber-reinforced polymer composites using 1D higher-order theories

M. Petrolo^{*,1}, A. Pagani², M. Trombini³, E. Carrera⁴

MUL² Lab, Department of Mechanical and Aerospace Engineering, Politecnico di Torino, Turin, Italy



ARTICLE INFO

Keywords:

Micromechanics
Voids
Statistical analysis
Carrera Unified Formulation

ABSTRACT

This work investigates the effect of voids within the matrix of composite materials. Effects on local stress and plastic strain values are evaluated by conducting a micromechanical analysis. The microscale Representative Volume Element (RVE) is modeled through refined 1D elements based on the Carrera Unified Formulation (CUF). Using 1D models for the RVE leads to a significant reduction in computational costs compared to standard 3D elements. Fibers are modeled as orthotropic, and the matrix has an elastoplastic behavior. Random distributions of voids are considered, and statistical analyses are carried out. Furthermore, the influence of the depth of the RVE is investigated. The results show significant mean and peak stress values increases as the void volume fraction grows. Also, the use of deeper RVE leads to higher stress values.

1. Introduction

Nowadays, fiber-reinforced composites are widely used in various engineering applications. Their advantages stem from the high specific strength and stiffness. However, the multiscale nature of composites requires the development of accurate models for analyzing their mechanical behavior (Aboudi et al., 2012) and achieving a level of accuracy comparable to that of isotropic materials. Another potentially critical aspect to consider is the generation of defects during manufacturing, e.g., dispersed air gaps – voids – in the matrix or the fiber misalignment. Such defects can alter the microstructure of composites, affect elastic properties, and trigger failure onset (Hinton et al., 2004). He et al. (2020) quantified voids within the composite while other works focused on countermeasures during manufacturing (Potter et al., 2008; Saenz-Castillo et al., 2019; Zhang et al., 2022). Moreover, several experimental works studied how the mechanical performance of fiber-reinforced polymers decays due to defects (Blok et al., 2018; Hsu, 1988; Justo et al., 2018; Stone and Clarke, 1975). Voids are most often considered among all defects due to their impact on various properties (Mehdikhani et al., 2019). The presence and shape of voids are critical in evaluating the homogenized properties of porous materials, as noted in Masmoudi et al. (2017) and Khdir et al. (2014). Additionally, voids can significantly modify the dimensions and configuration of the stress field within the material (Touliatou and Wheel, 2019).

The numerical modeling of defects aims to understand better the performance degradation of composites (Talreja, 2015). Numerical methods to estimate material properties usually involve analysis of a Representative Volume Element (RVE) (Sun and Vaidya, 1996). The RVE is considered the smallest representative volume and corresponds to a periodic fiber packing sequence (Li and Sitnikova, 2019; Gitman et al., 2007; Gitman, 2006). Micromechanics is used to evaluate the behavior of multiphase materials (Aboudi et al., 2012; Aboudi, 2004; Nemat-Nasser and Hori, 1999), and various approaches are available for obtaining homogenized properties, and local stress and strain fields (Aboudi et al., 2001). Among the others, the method of cells has proven to be very versatile and reliable (Aboudi, 1981) and was later extended (Aboudi, 2004, 1989; Paley and Aboudi, 1992). The Generalised Method of Cells (GMC) was used by Dai et al. (2022) to simulate the effect of residual thermal stress and weak interphases on micro-cracking and later progressive failure of B₄C-TiB₂ composites. In some recent works, the High-Fidelity Generalised Method of Cells (HFGMC) replaced the GMC as a new generalized method (Aboudi, 2004; Bednarczyk et al., 2010; Pineda, 2012; Pineda et al., 2013). Recent investigations (Huang, 2023b,a) examined the effect of reinforcement-induced stress concentration on homogenized stress in the matrix by incorporating a stress concentration factor (SCF).

* Correspondence to: MUL² Lab, Department of Mechanical and Aerospace Engineering, Politecnico di Torino, Corso Duca degli Abruzzi 24, 10129 Torino, Italy.
E-mail addresses: marco.petrolo@polito.it (M. Petrolo), alfonso.pagani@polito.it (A. Pagani), mattia.trombini@polito.it (M. Trombini), erasmo.carrera@polito.it (E. Carrera).

¹ Associate Professor.

² Associate Professor.

³ PhD Student.

⁴ Professor

The Finite Element Method (FEM) is another approach for micromechanics. In the work of [Dong and Huo \(2016\)](#), FEM was used to model voids and dry patches via a two-scale RVE model with periodic boundary conditions to evaluate elastic constants and micro stress of 3D braided composites. [Huang and Gong \(2018\)](#) discussed the influence of voids in fiber tows and woven composites. They used multiscale FEM and found that the reduction of elastic properties in woven composites is less sensitive to the voids in the matrix than those in fiber tows. [Jiang et al. \(2019\)](#) showed that voids have little influence on the longitudinal stress-strain response, while a more pronounced decrease of in-plane and out-of-plane shear strength with increasing voids content is obtained. In [Pineda et al. \(2022\)](#), the prediction of the difference in strength between a baseline model of a woven composite containing 0.4% of voids and a representative model with ten times increase in void content was obtained using the NASA Multiscale Analysis Tool (NASMAT). A ~10%–11% variation between the two models in the ultimate stress was found. The effect of interfiber and circular voids on the strength of composite under transverse tension and compression was discussed in [Ashouri Vajari et al. \(2014\)](#), while [Zhang et al. \(2021\)](#) investigated the irregular stress and damage evolution contours that occur due to the random arrangement of the fibers and the voids in the matrix. In the work of [Carrera et al. \(2020\)](#), the effect of matrix voids on homogenized properties was studied. Moreover, dehomogenization allowed for obtaining local stress fields using both random and clustered distributions of voids. [Nagaraj et al. \(2021\)](#) introduced the material nonlinearity by involving an elastoplastic matrix behavior and studied how voids affect von Mises stress (VM) and the equivalent plastic strain (PEEQ) of composites.

To improve accuracy, 3D FEM is used for RVE; however, such a strategy may lead to unaffordable computational costs in many cases, e.g., multiscale and nonlinear analyses. An alternative approach to tackling such a problem was proposed by [Carrera et al. \(2014\)](#), [Kaleel et al. \(2017, 2018b\)](#) and based on the use of 1D higher-order structural theories obtained via the Carrera Unified Formulation (CUF). The present article adopts such a framework to reduce computational costs while maintaining 3D accuracy in stress and strain. Following this approach, shape functions act along the RVE axis, and the expansion functions enhance the cross-section kinematics. Past works proved that 1D CUF could be used to tackle various problems, including progressive failure analysis ([Pagani et al., 2022](#)) and composite stress analysis.

This work aims to extend the findings from [Carrera et al. \(2020\)](#), including the effect of matrix nonlinearity, as previously done by [Nagaraj et al. \(2021\)](#), where a single random distribution of voids is used for each strain applied. The present paper involves micromechanical dehomogenization, followed by a statistical analysis performed on multiple void distributions. The purpose is to collect statistical parameters and identify critical load conditions for the RVE, leading to stress peaks. Furthermore, the present work investigates the impact of the RVE thickness on the micromechanical nonlinear response. This paper is organized as follows: Section 2 presents the CUF approach; Section 3 describes the micromechanics model; Section 4 provides a brief overview of the statistical analysis and corresponding parameters; in Section 5 numerical results are shown and discussed; and in Section 6 conclusions are drawn.

2. CUF and finite element formulation

Considering the reference frame shown in [Fig. 1](#), the three displacement components are

$$\mathbf{u}(x, y, z) = \{u_x, u_y, u_z\}^T \quad (1)$$

CUF is employed to generate structural theories and related equations. In the 1D case, the displacement field becomes

$$\mathbf{u}(x, y, z) = F_\tau(x, z) \mathbf{u}_\tau(y), \quad \tau = 1, 2, \dots, M \quad (2)$$

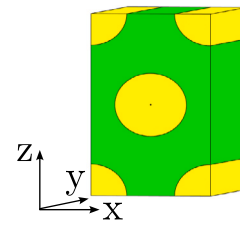


Fig. 1. Reference frame.

F_τ is the expansion function and \mathbf{u}_τ is the vector of generalized displacements. Moreover, M is the number of expansion terms. The expansion exploits Lagrange polynomials in this work, resulting in a Component Wise (CW) approach. A comprehensive explanation of Lagrange polynomials for CUF can be found in [Carrera and Petrolo \(2012\)](#). The current work utilizes 9-node bi-quadratic expansion elements (L9) to discretize the unknown displacements over the cross-section, as shown in [Fig. 2](#). The iso-parametric formulation is used to model arbitrarily shaped geometries. The L9 displacement field is given by

$$\begin{aligned} u_x &= F_1 u_{x_1} + F_2 u_{x_2} + F_3 u_{x_3} + \dots + F_9 u_{x_9} \\ u_y &= F_1 u_{y_1} + F_2 u_{y_2} + F_3 u_{y_3} + \dots + F_9 u_{y_9} \\ u_z &= F_1 u_{z_1} + F_2 u_{z_2} + F_3 u_{z_3} + \dots + F_9 u_{z_9} \end{aligned} \quad (3)$$

u_{x_1}, \dots, u_{z_9} are the displacement variables of the problem, and they represent the translational displacement components of each point of the L9 element.

The beam is discretized using the classical finite element approach along y using standard shape functions, i.e.,

$$\mathbf{u}(x, y, z) = F_\tau(x, z) N_i(y) \mathbf{u}_{\tau i}, \quad \tau = 1, 2, \dots, M, \quad i = 1, 2, \dots, p + 1 \quad (4)$$

N_i is the shape function of order p , and $\mathbf{u}_{\tau i}$ is the vector of nodal displacements. This paper used CUF to obtain 1D structural models, with standard shape functions acting along one direction and expansion functions over the cross-section. The three displacement components are obtained as a combination of generalized displacement variables, such variables are the nodal degrees of freedom of the problem. If, for instance, an expansion with five terms is used, the number of nodal degrees of freedom is fifteen. As mentioned in the book of [Washizu \(1968\)](#), 1D or 2D models with infinite expansions provide 3D solutions. A convergence analysis over the expansion terms can be carried out to select the proper order. Also, the role of each term over the solution can be studied via the axiomatic/asymptotic approach ([Carrera and Petrolo, 2010](#)). In recent years, CUF has been applied to many classes of composite structures, different loading conditions, and dynamic and nonlinear regimes ([Carrera et al., 2021](#)). The stress and strain components are

$$\begin{aligned} \boldsymbol{\sigma} &= \{\sigma_{xx} \ \sigma_{yy} \ \sigma_{zz} \ \sigma_{xy} \ \sigma_{xz} \ \sigma_{yz}\}^T \\ \boldsymbol{\varepsilon} &= \{\varepsilon_{xx} \ \varepsilon_{yy} \ \varepsilon_{zz} \ \varepsilon_{xy} \ \varepsilon_{xz} \ \varepsilon_{yz}\}^T \end{aligned} \quad (5)$$

The linear strain-displacement relation is used,

$$\boldsymbol{\varepsilon} = \mathbf{D} \mathbf{u} \quad (6)$$

\mathbf{D} is the linear differential operator, i.e.,

$$\mathbf{D} = \mathbf{D}_\Omega + \mathbf{D}_y$$

$$\mathbf{D}_\Omega = \begin{bmatrix} \frac{\partial}{\partial x} & 0 & 0 \\ 0 & 0 & 0 \\ 0 & 0 & \frac{\partial}{\partial z} \\ 0 & \frac{\partial}{\partial x} & 0 \\ \frac{\partial}{\partial z} & 0 & \frac{\partial}{\partial x} \\ 0 & \frac{\partial}{\partial z} & 0 \end{bmatrix} \quad \mathbf{D}_y = \begin{bmatrix} 0 & 0 & 0 \\ 0 & \frac{\partial}{\partial y} & 0 \\ 0 & 0 & 0 \\ \frac{\partial}{\partial y} & 0 & 0 \\ 0 & 0 & 0 \\ 0 & 0 & \frac{\partial}{\partial y} \end{bmatrix} \quad (7)$$

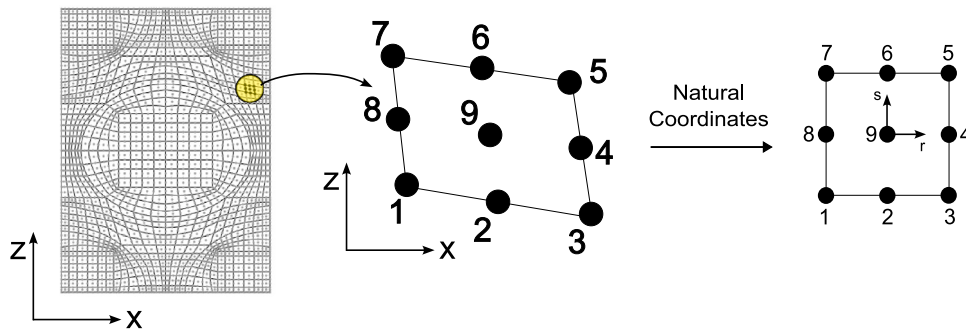


Fig. 2. L9 expansion in natural coordinates.

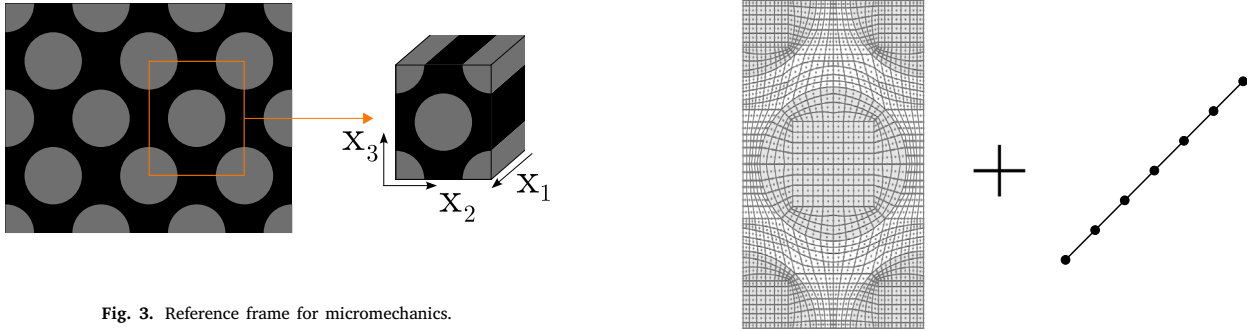


Fig. 3. Reference frame for micromechanics.

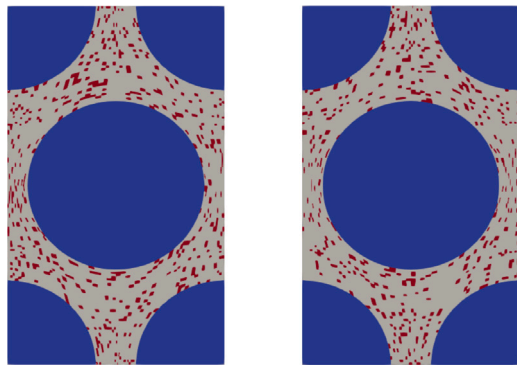


Fig. 4. Two different sets of void distribution over the section of the hex-packed RVE - 5% of void volume fraction.

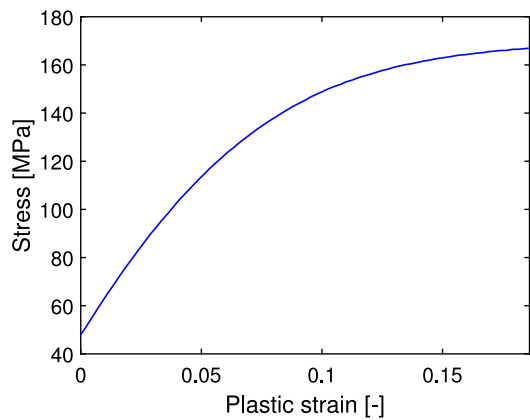


Fig. 5. Plasticity curve of the matrix.

Fig. 6. Hex-Pack 1D model using CUF.

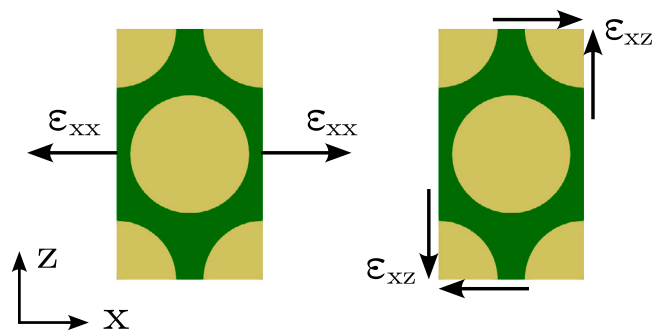


Fig. 7. Axial (left) and shear (right) strains applied to the hex-packed RVE.

The constitutive law is, then, employed,

$$\sigma = C^{ep} \epsilon \tag{8}$$

C^{ep} is the elastoplastic tangent matrix. This work considers material nonlinearities due to von Mises plasticity, and a Newton–Raphson scheme is used to solve the iterative process. Using the principle of virtual work over strain energy and the work of external forces,

$$\delta L_{int} = \delta L_{ext} \tag{9}$$

Defining V as the volume of the body, the strain energy becomes

$$\delta L_{int} = \delta u_{sj} k_{\tau sij} u_{\tau i} \tag{10}$$

$k_{\tau sij}$ is the Fundamental Nucleus (FN),

$$k_{\tau sij} = \int_V \mathbf{D}_{sj}^T C^{ep} \mathbf{D}_{\tau j} dV \tag{11}$$

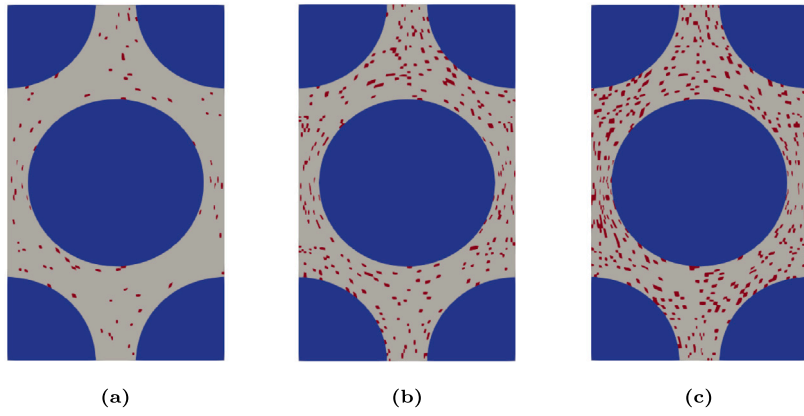


Fig. 8. Distribution of voids over the section of the hex-packed RVE - 1% (a), 3% (b), and 5% (c).

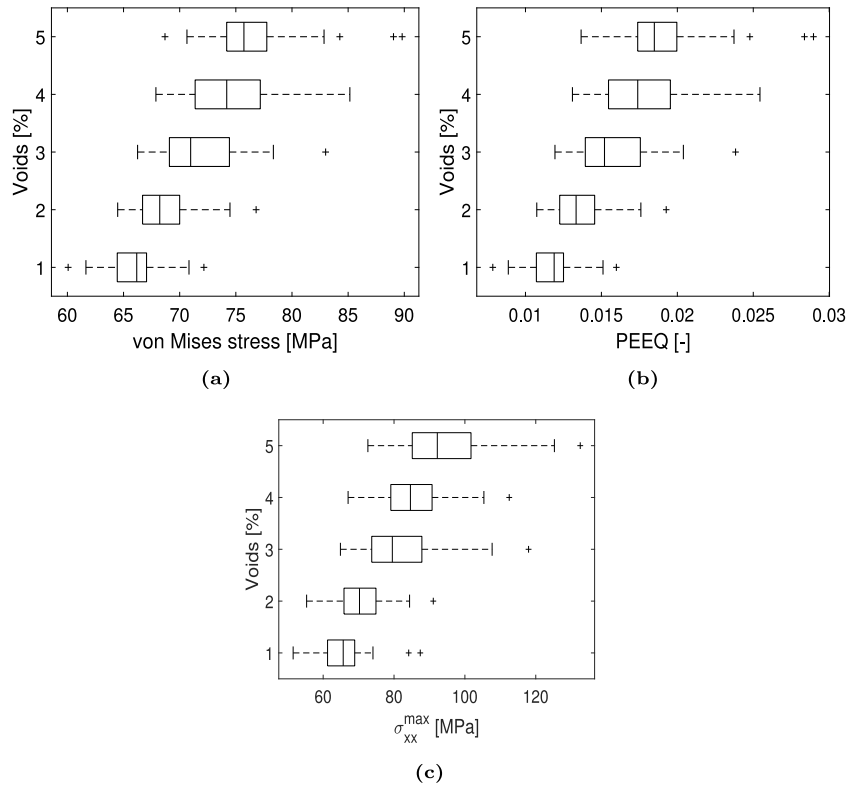


Fig. 9. Boxplots of von Mises stress (a), maximum equivalent plastic strain (b), and maximum σ_{xx} (c) over the matrix of hex-packed RVE when ϵ_{xx} is applied.

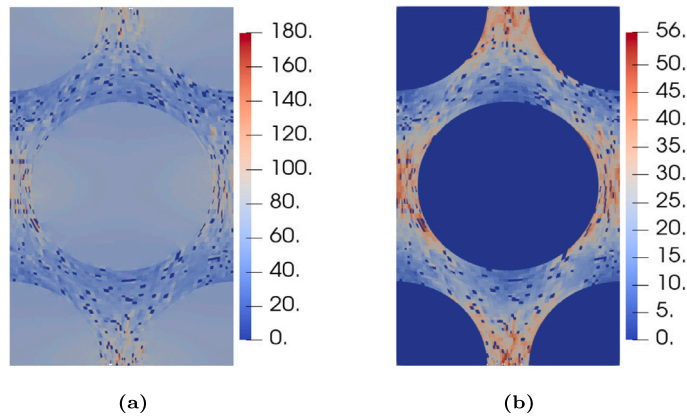


Fig. 10. Distribution of σ_{xx} (a) and von Mises stress (b) over the cross-section of hex-packed RVE with 5% of voids when ϵ_{xx} is applied, MPa.

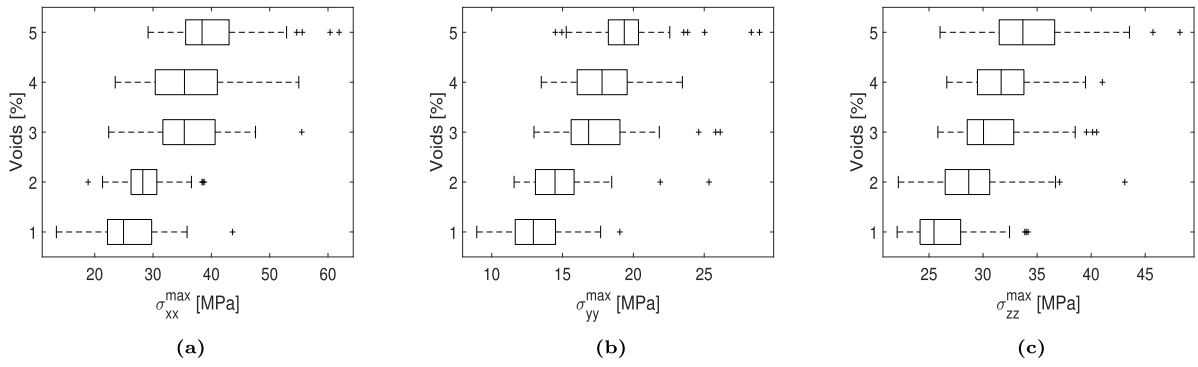


Fig. 11. Boxplots of maximum σ_{xx} (a), σ_{yy} (b), and σ_{zz} (c) over the fiber of hex-packed RVE when ϵ_{xz} is applied.

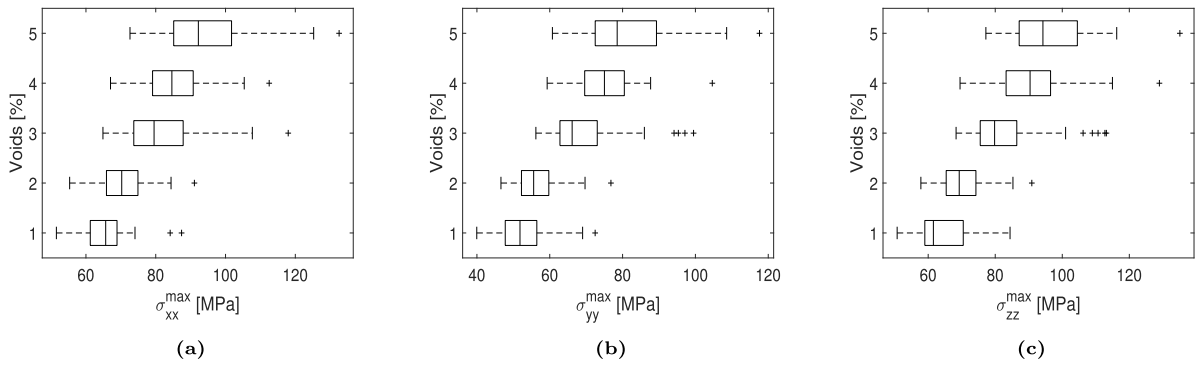


Fig. 12. Boxplots of maximum σ_{xx} (a), σ_{yy} (b), and σ_{zz} (c) over the matrix of hex-packed RVE when ϵ_{xz} is applied.

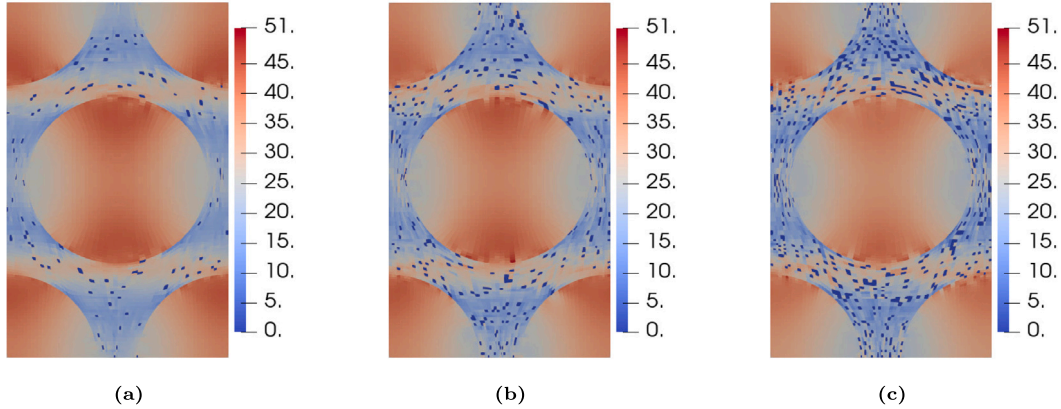


Fig. 13. Distribution of σ_{xz} over the cross-section of hex-packed RVE with 1% of voids (a), 3% of voids (b), and 5% of voids (c) when ϵ_{xz} is applied, MPa.

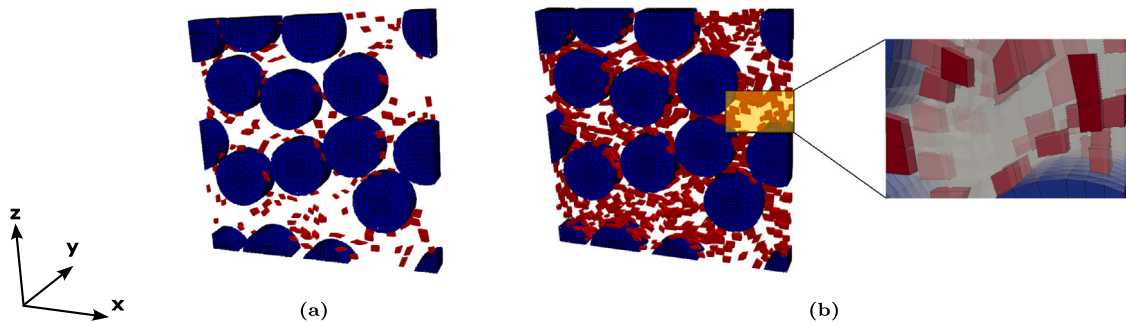


Fig. 14. Void distributions over the RVE with randomly distributed fibers: 1% (a) and 5% (b), with a magnification of void dispersion.

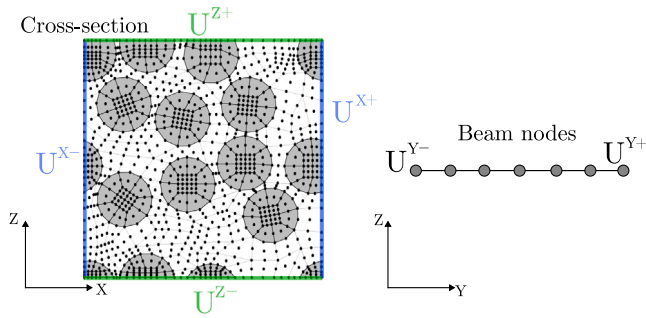


Fig. 15. Application of PBC on the random RVE on both the cross-section and the nodes in the y -direction.

FN is a 3×3 matrix composed by

$$k_{\tau sij} = \begin{bmatrix} k_{\tau sij}^{xx} & k_{\tau sij}^{xy} & k_{\tau sij}^{xz} \\ k_{\tau sij}^{yx} & k_{\tau sij}^{yy} & k_{\tau sij}^{yz} \\ k_{\tau sij}^{zx} & k_{\tau sij}^{zy} & k_{\tau sij}^{zz} \end{bmatrix} \quad (12)$$

Similarly, the external force work can be obtained as follows:

$$\delta L_{\text{ext}} = \delta u_{sj} p_{sj} \quad (13)$$

p_{sj} is the external load vector. By iterating indices τ, s, i, j , the global stiffness matrix and global load vector are built. For the sake of brevity, the explicit expression of FN are not reported here, but can be found in Carrera et al. (2014).

3. Micromechanics framework

The reference frame adopted to describe the micromechanical framework is shown in Fig. 3. This work involves different types of representative volume elements, the beam model is used along x_1 , while L9 defines the displacement fiend over the x_2 - x_3 plane. Periodic boundary conditions (PBC) are employed (Xia et al., 2003) as follows:

$$u_i^{j+}(x, y, z) - u_i^{j-}(x, y, z) = \bar{\epsilon}_{ik} \Delta x_k^j \quad (14)$$

$$\Delta x_k^j = x_k^{j+} - x_k^{j-}$$

$j+$ and $j-$ indicate the positive and negative x_k -directions. $\bar{\epsilon}_{ik}$ is the applied macroscopic strain. The homogenized strain ($\bar{\epsilon}_{ij}$) and stress ($\bar{\sigma}_{ij}$) can be evaluated by volume averaging the microscopic strain (ϵ_{ij}) and stress (σ_{ij}) (Sun and Vaidya, 1996),

$$\bar{\epsilon}_{ij} = \frac{1}{V} \int_V \epsilon_{ij} dV \quad (15)$$

$$\bar{\sigma}_{ij} = \frac{1}{V} \int_V \sigma_{ij} dV \quad (16)$$

By introducing the homogenized material matrix \bar{C}_{ijkl} , the constitutive relation can be expressed as follows:

$$\bar{\sigma}_{ij} = \bar{C}_{ijkl} \bar{\epsilon}_{kl} \quad (17)$$

More details concerning the CUF micromechanics framework can be found in Kaleel et al. (2017).

Voids are modeled by randomly selecting a set of Gauss points within the matrix domain and assigning them low elastic moduli, as previously done in Carrera et al. (2020) and Nagaraj et al. (2021). The computation of the FE matrices employs the Gauss-Legendre quadrature, and the void sites' Gauss points concur to the integrals with modified elastic moduli. The random selection of matrix Gauss points as void sites is carried out to reach a given void volume fraction is reached. This process generates voids with a domain size equal to the volume associated with the selected Gauss point, not the entire element, and distinct sets of Gauss point combinations can provide the same

total void volume fraction. In the computation of the FE matrices, Gauss points that are void sites are considered with modified elastic properties. Fig. 4 presents an illustrative case of different Gauss point selections with a void volume fraction of 5%.

4. Statistical analysis

The novelty proposed in this article involves the extension of the effect of voids on composites that also exhibit a plastic behavior. For each void volume fraction, 50 defect distributions were randomly generated. The number of distributions was chosen as a reasonable compromise between the computational cost of non-linear elastoplastic analysis and the need for sufficient results to perform statistical analysis (Carrera et al., 2020). The aim of this Section is the introduction of statistical parameters used in this paper to investigate the effect of random void distributions on the mechanical response of the RVE. Absolute maximum and minimum of each mechanical quantity for each distribution of results were considered. Furthermore, the mean value and standard deviation (s) were considered,

$$s = \sqrt{\frac{1}{50-1} \sum_{i=1}^{50} |x_i - \bar{x}|^2} \quad (18)$$

x_i is a given mechanical quantity and \bar{x} is the mean value of each distribution. Also, the analysis considered the first, second and third quartiles. As well-known, the second quartile q_2 is the median; the first quartile q_1 is the median of the bottom half and the third quartile q_3 is the median of the top half (Langford, 2006). For the sake of clarity, a graphic representation of statistical parameters was used via boxplots in which quartiles, the notch extremes and the outliers can be observed. The notch extremes represent interval endpoints and they are computed as follows:

$$q_L = q_2 - 1.57 \frac{q_3 - q_1}{\sqrt{50}} \quad (19)$$

$$q_U = q_2 + 1.57 \frac{q_3 - q_1}{\sqrt{50}} \quad (20)$$

q_L is the lower endpoint, and q_U the upper one. Values exceeding the endpoints are the outliers,

$$q < q_L \quad \& \quad q > q_U \quad (21)$$

5. Numerical results

Numerical results considered two RVE architectures, hex-packed and randomly distributed fibers, and the influence of various parameters, such as the void volume fraction and the depth of the RVE. Void volume fractions from 1 to 5% were considered. As a matter of clarity, implementing a fiber-dispersed RVE does not contrast with the conceptualization of periodicity. Real composite microstructures are rarely structured; consequently, classical periodic unit cells (PUC) may not provide precisely the microstructural parameters (Li et al., 2018). In addition, microstructure conditions, such as the dimensions, geometry, spatial distribution, and material properties, strongly influence the interactions between the constituents and thus play a decisive role in the performance of these composites at a multiscale level (Li et al., 2018; Park et al., 2019). Therefore, a random packaging of fibers results in more attractive detection of the local response of composites. In addition, the material nonlinearity was considered for the matrix using the J2 flow theory as detailed in Carrera et al. (2019). The flow theory, referred to as the von Mises plasticity model, is based on the hypothesis that an isotropic material yields when the J2 stress deviator reaches the critical value. The following equation states an isotropic hardening case

$$f = q(\sigma) - \sigma_y(\bar{\epsilon}_p) \quad (22)$$

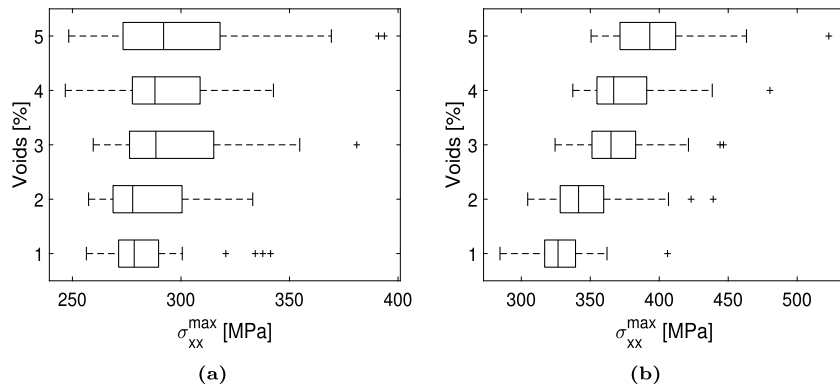


Fig. 16. Boxplots of maximum σ_{xx} over the fiber (a) and in matrix (b) of random RVE when ϵ_{xx} is applied.

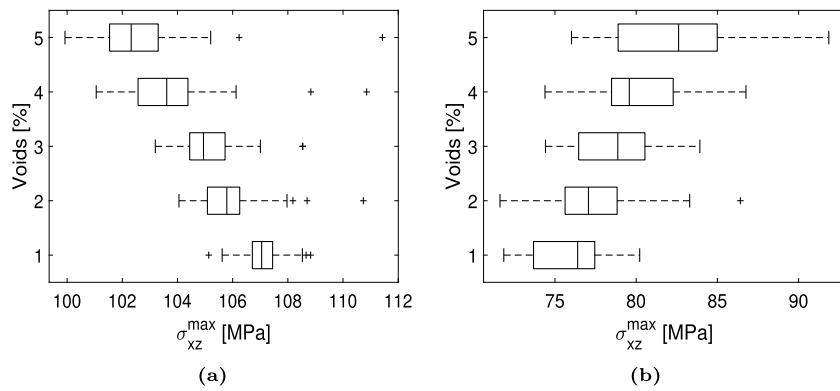


Fig. 17. Boxplots of maximum σ_{xz} over the fiber (a) and matrix (b) of random RVE when ϵ_{xz} is applied.

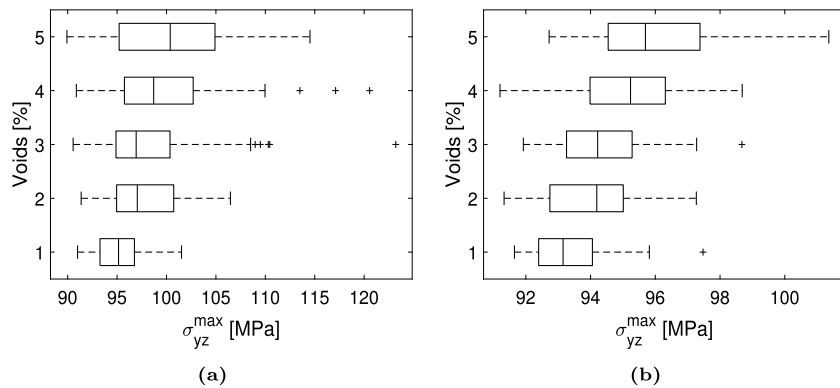


Fig. 18. Boxplots of maximum σ_{yz} over the fiber (a) and matrix (b) of random RVE when ϵ_{yz} is applied.

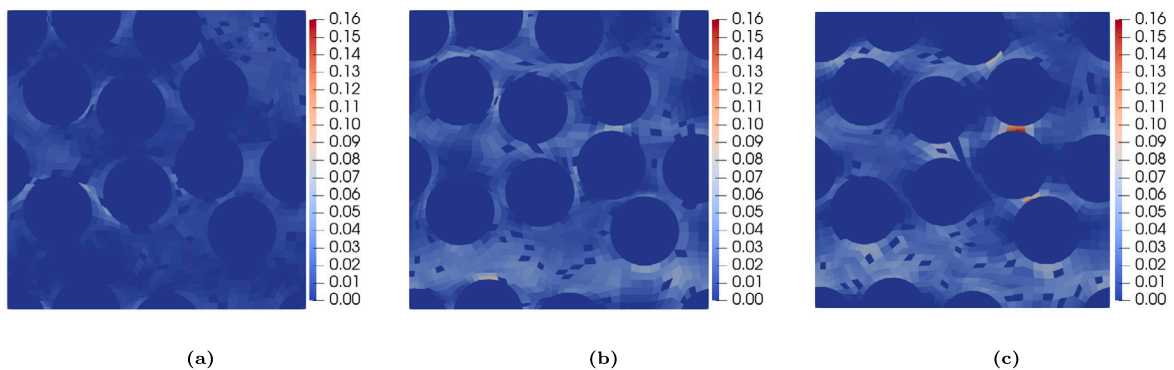


Fig. 19. Distribution of PEEQ over the cross-section of random RVE with 3% of voids when ϵ_{xx} (a), ϵ_{xz} (b), and ϵ_{yz} (c) are applied.

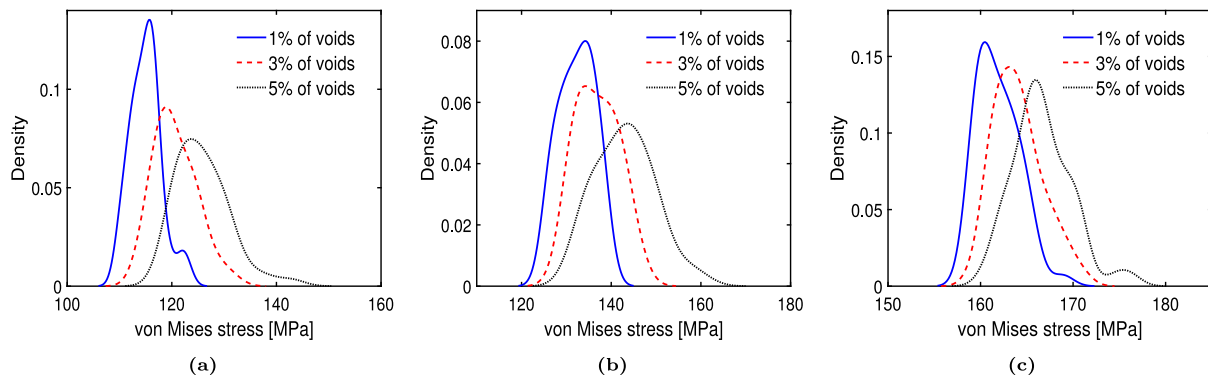


Fig. 20. Probability density function of VM in the random RVE with 3% of voids when ϵ_{xx} (a), ϵ_{xz} (b), and ϵ_{yz} (c) are applied.

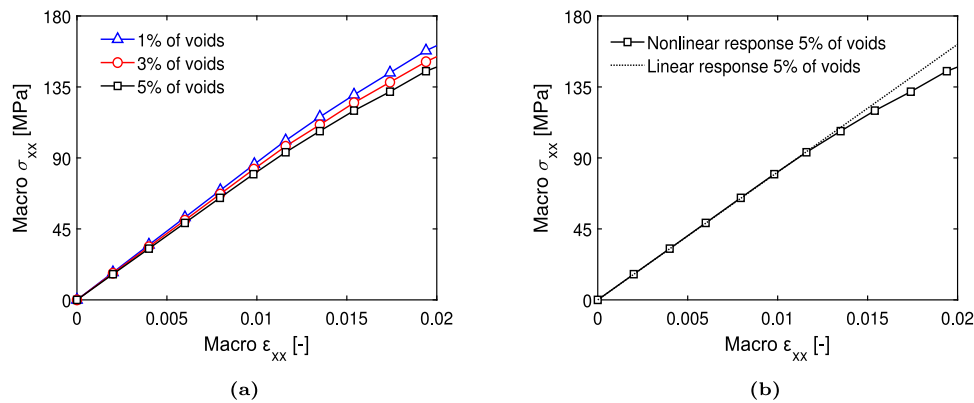


Fig. 21. Macroscopic stress–strain response (a) and comparison between nonlinear and linear curves with 5% of voids (b) for the random RVE when ϵ_{xx} is applied.

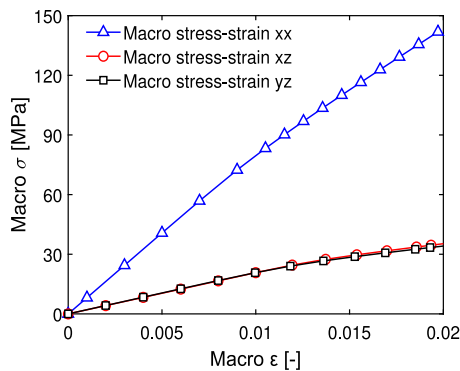


Fig. 22. Comparison of the nonlinear homogenized stress–strain response for the random RVE with 5% of void under different load conditions.

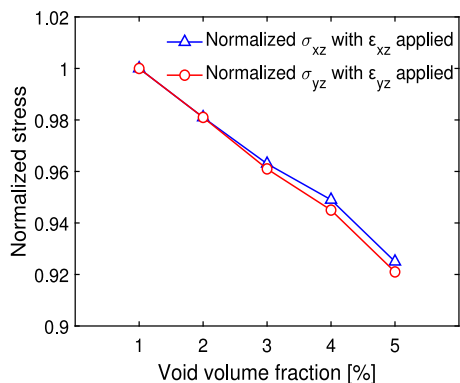


Fig. 23. Effect of voids on normalized macroscopic response for the random RVE.

where f is the von Mises locus, σ_y is the yield stress, $\bar{\epsilon}_p$ is the isotropic hardening parameter and $q(\sigma)$ is the von Mises stress, composed by

$$q(\sigma) = \sqrt{3J_2} = \sqrt{\frac{1}{2} \left[(\sigma_{xx} - \sigma_{yy})^2 + (\sigma_{yy} - \sigma_{zz})^2 + (\sigma_{zz} - \sigma_{xx})^2 + 6(\sigma_{xy}^2 + \sigma_{xz}^2 + \sigma_{yz}^2) \right]} \quad (23)$$

where J_2 is the second invariant of the deviatoric stress. In the present framework, a rate-independent isotropic hardening is employed. It is included in the formulation by defining the yield stress as a function of the accumulated plastic strain, as shown in Eq. (22). This corresponds to a uniform expansion of the initial yield locus. The strain hardening approach is also utilized in the current framework to address the isotropic hardening behavior. The framework accommodates data points that approximate the arbitrarily nonlinear hardening curve. A linear interpolation is employed between data points to enable the direct use of the experimental hardening curve within the simulation. The constitutive model implemented within the CUF framework is based on (Neto et al., 2008).

5.1. Statistical analysis on hex-packed RVE

The aim of this section is the statistical analysis of local stress components through dehomogenization on a hex-packed RVE with 60% of fiber volume fraction. The mechanical properties of fibers and matrix are listed in Table 1, and the nonlinear behavior of the matrix is described using a plasticity curve, as illustrated in Fig. 5. The cross-section has 920 L9 elements, whereas 2 B4 elements were used along the y -direction, as shown in Fig. 6. The number of L9 and B4 elements was chosen according to the convergence analysis carried out in Carrera et al. (2020). Axial and shear strains equal to 0.005 were applied, as shown in Fig. 7. Fig. 8 shows the void distributions adopted.

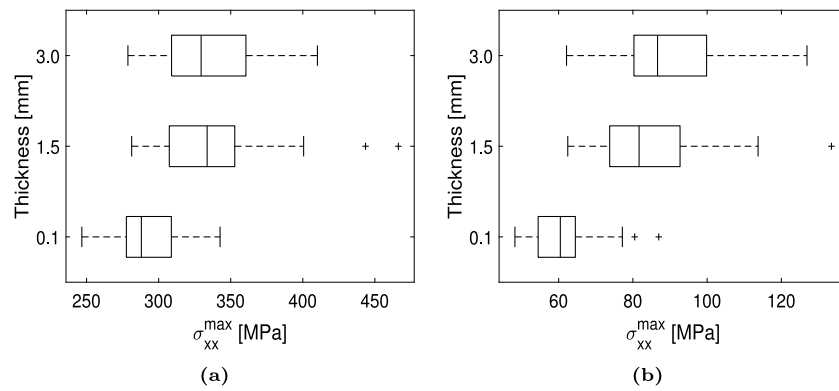


Fig. 24. Boxplots of maximum σ_{xx} in the fiber of random RVE with variable thickness when ϵ_{xx} (a) and ϵ_{xz} (b) are applied.

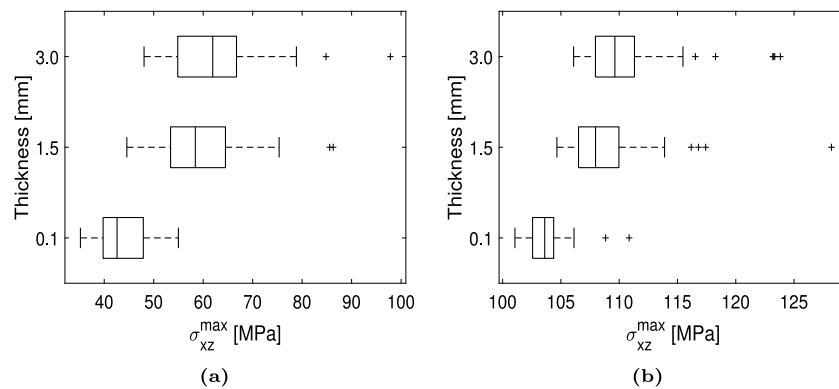


Fig. 25. Boxplots of maximum σ_{xz} in the fiber of the random RVE with variable thickness when ϵ_{xx} (a) and ϵ_{xz} (b) are applied.

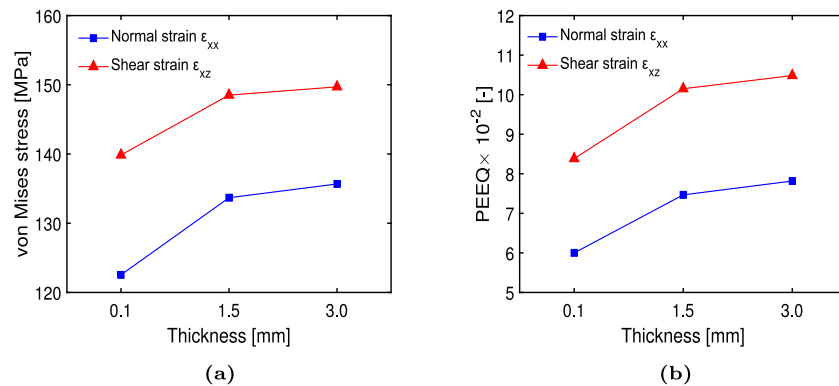


Fig. 26. Mean VM (a) and PEEQ (b) in the random RVE for various thickness values.

Table 1
Elastic mechanical properties of constituent materials - elastic and shear moduli in GPa.

Fiber	E_{11}	E_{22}	E_{33}	G_{12}	G_{13}	G_{23}	ν_{12}	ν_{13}	ν_{23}
Fiber	276.00	16.00	16.00	5.00	5.00	5.00	0.28	0.28	0.31
Matrix	E	ν							
Matrix	3.50	0.35							

The statistical analysis uses the parameters defined in Section 4 for each void distribution. Considering the axial strain as the load case, Table 2 presents the statistical parameters for maximum stress components for different void volume fractions Fig. 9 shows boxplots concerning the von Mises stress (VM), equivalent plastic strain (PEEQ), and maximum σ_{xx} over the matrix. Table 3 presents statistical parameters concerning stress and strain components over the matrix, whereas Fig. 10 shows the distributions of σ_{xx} and von Mises stress

over the cross-section with 5% of void volume fraction. Shear strain is then considered, and boxplots related to the maximum normal stress over the fiber and the matrix are shown in Figs. 11 and 12. Table 4 contains the statistical parameters concerning VM and PEEQ over the matrix for each void volume fraction. Furthermore, Fig. 13 compares the final distribution of local σ_{xz} over the cross-section for increasing void percentages. The results show that:

Table 2
Statistical parameters of stress components (MPa) over the fiber of hex-packed RVE when ϵ_{xx} is applied.

	\bar{x}	s	min	max	q ₁	q ₂	q ₃	Voids [%]
σ_{xx}^{max}	85.211	3.385	81.068	101.582	82.777	84.494	86.841	1
	87.640	4.325	81.376	102.303	84.741	86.942	88.618	2
	88.639	4.426	82.017	104.892	85.624	87.588	89.992	3
	91.100	6.540	82.066	115.349	86.632	89.261	95.073	4
	93.109	7.652	82.118	117.803	87.653	90.346	97.089	5
σ_{yy}^{max}	33.260	1.474	30.860	36.344	31.998	33.274	34.317	1
	35.710	2.354	32.174	41.451	34.176	35.000	37.011	2
	37.207	3.440	32.815	48.407	34.478	36.783	38.430	3
	37.519	2.759	32.396	44.224	35.381	36.832	39.837	4
	39.338	3.410	33.620	46.777	36.945	38.989	42.155	5
σ_{zz}^{max}	41.858	2.950	38.196	53.227	39.855	41.398	42.937	1
	43.890	4.062	38.559	54.474	40.959	42.609	45.246	2
	46.194	3.400	40.244	54.712	44.111	45.842	48.301	3
	47.766	6.319	40.247	71.726	43.747	46.070	50.173	4
	48.493	4.499	42.231	60.163	45.136	47.673	50.055	5

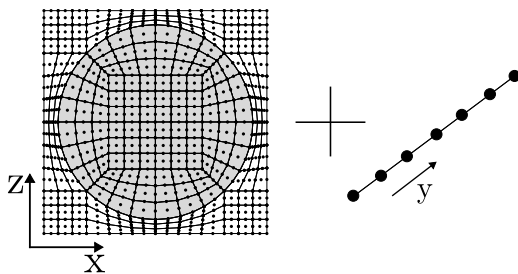


Fig. 27. Square-packed architecture 1D model using CUF.

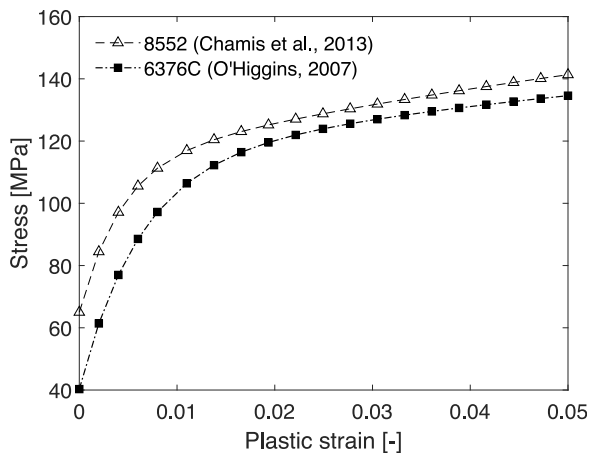


Fig. 28. Plasticity curves for the 8552 matrix (Chamis et al., 2013) and for the 6376C (O'Higgins, 2007).

- Almost all stress and strain components increase as the void volume fraction grows. The impact of the void volume fraction is higher on the matrix than the fiber.
- The shear load case leads to a more severe increment of von Mises stress and equivalent plastic strain with increasing voids compared to the axial case.

- The presence of voids can alter the stress distributions significantly, with variations in mean values of stress components larger than 10%.

5.2. Statistical analysis on RVE with randomly distributed fibers

The second RVE architecture, based on the work of Pineda et al. (2013), has a random distribution of fibers and a volume fraction of 47%, with properties provided in Table 1 and the elastoplastic behavior of the matrix is detailed in Fig. 5. Two B4 elements along the y -direction and 277 L9 over the cross-section were used as previously done in Nagaraj et al. (2021). The magnitude of applied strains is 0.02. In addition, voids were dispersed within the matrix, as shown in Fig. 14 for two void volume fractions, and the application of PBC on the RVE is discernible in Fig. 15.

Figs. 16–18 show the boxplots of axial and shear transverse stresses. Table 5 presents mean values of normal stresses, VM, and PEEQ. Table 6 shows the variation of the mean value as compared to the minimum and maximum, e.g., σ_{xx} mean value when ϵ_{xx} is applied is 18.4% higher than the minimum value and 14.7% lower than the maximum. Table 7 presents the maximum values of shear stresses. Fig. 19 compares the distribution of PEEQ over the section for various loading conditions and 3% of voids, and Fig. 20 shows the probability density function (Haynes, 2013) of VM. Finally, homogenization is performed to obtain the macroscopic behavior of the RVE, and Fig. 21 illustrates the macroscopic stress–strain curve for the RVE loaded in the x -direction with increasing void volume fractions, also exhibiting a comparison between the linear and nonlinear response of the RVE. In Fig. 22, the homogenized stress–strain curves are presented for the random RVE that comprises 5% of void under (i) axial strain ϵ_{xx} ; (ii) shear strain ϵ_{xz} ; (iii) shear strain ϵ_{yz} . Furthermore, assuming the macroscopic stress determined at 1% of voids as the reference, Fig. 23 illustrates the influence that voids have on normalized stress for the RVE loaded with shear strains ϵ_{xz} and ϵ_{yz} .

The results suggest that:

- As in the previous Section, an increase in void fraction leads to higher stresses.
- The range of stress values at a given void fraction is around 30%.
- Ranging from 1 to 5% of voids, the VM mean value increases by some 5%–10%.
- The presence of voids has a relevant effect also on the macroscopic response of the RVE. Specifically, higher void fractions lead to a decrease in the macroscopic stress.

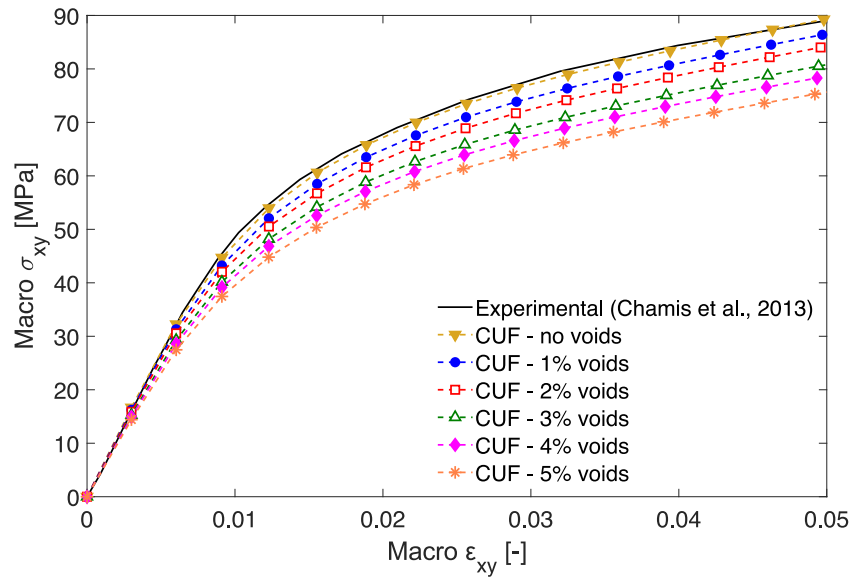


Fig. 29. Nonlinear homogenized stress–strain response for the pristine square-packed RVE and with void content from 1 to 5% and comparison with reference benchmark (Chamis et al., 2013) of IM7-8552 material system.

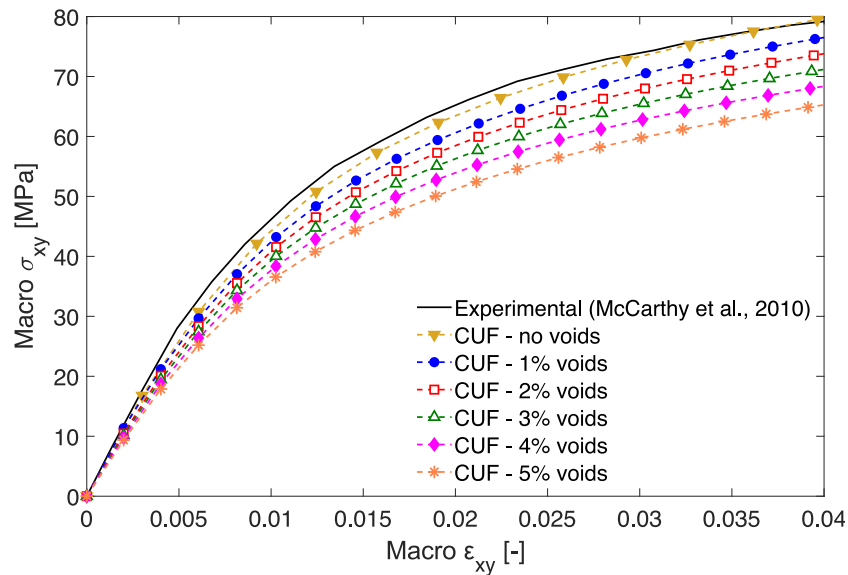


Fig. 30. Nonlinear homogenized stress–strain response for the pristine square-packed RVE and with void content from 1 to 5% and comparison with reference benchmark (McCarthy et al., 2010) of HTA-6376C material system.

5.3. Influence of the RVE thickness on stress and plastic strain distributions

This section investigates the influence of the RVE thickness along the fiber direction on the micromechanical response. As the defects are randomly located within the matrix (Mehdikhani et al., 2019), their distribution through the thickness of the RVE may induce significant variations in the peaks of the local stress and strain. The void volume fraction is 4% for all cases, and the thickness varies from 0.1 to 3 mm; all other properties are as in Section 5.2. Figs. 24 and 25 show boxplots for σ_{xx} and σ_{xz} , whereas, Fig. 26 compares mean von Mises stress and PEEQ when the thickness varies from 0.1 to 3.0 mm. The results show that:

- Higher thickness values lead to higher σ_{xx} and σ_{xz} , and VM.
- The variation of VM is in the range 5%–10% if considering 0.1 and 3 mm thickness values. The same variation is very low if the thickness changes from 1.5 to 3 mm.

5.4. Influence of voids on the homogenized response

The current section investigates voids’ influence on composites’ macroscopic stress–strain response. The selected architecture is a square-packed RVE under a shear strain ϵ_{xy} . The discretization consists of 216 L9 elements for the cross-section, while 2 B4 elements act along the fiber direction, as shown in Fig. 27. The accuracy of CUF findings compared to the experimental references has been assessed in Kaleel et al. (2018a), where no voids were considered. This work compares the results of the current micromechanical model to some experimental benchmarks with a pristine RVE. After that, the investigation focuses on the macroscopic response with void content ranging from 1 to 5%. The current assessment involves two different material systems, namely (i) IM7-8552 with a 60% of fiber volume fraction (Chamis et al., 2013), (ii) HTA-6376C with a 62% of fiber volume fraction (O’Higgins, 2007; McCarthy et al., 2010). The material properties of the constituents are listed in Table 8, whereas Fig. 28 presents the plasticity curves for the

Table 3
Statistical parameters of stress (MPa) and strain components over the matrix of hex-packed RVE when ϵ_{xx} is applied.

	\bar{x}	s	min	max	q ₁	q ₂	q ₃	Voids [%]
σ_{xx}^{max}	141.737	11.330	122.317	173.051	134.401	141.080	147.609	1
	161.398	14.053	137.267	192.493	151.342	159.667	173.113	2
	177.801	19.021	151.964	249.867	165.521	171.407	185.255	3
	197.592	29.211	157.275	320.815	180.166	191.493	212.010	4
	206.194	16.934	180.313	248.496	191.924	203.469	216.301	5
σ_{yy}^{max}	94.719	9.971	77.610	122.005	87.862	94.132	99.723	1
	111.920	12.046	90.939	139.048	102.965	110.674	121.943	2
	126.130	16.587	103.782	189.439	115.842	120.507	132.349	3
	143.406	25.658	107.763	251.565	127.674	137.509	156.491	4
	150.898	14.798	128.256	188.180	138.909	149.439	159.479	5
σ_{zz}^{max}	88.838	9.388	71.600	113.499	82.347	87.788	94.303	1
	106.108	12.530	83.451	135.423	95.672	103.491	115.861	2
	119.343	16.434	95.155	184.986	107.710	114.347	125.966	3
	137.292	26.006	92.805	243.959	120.776	131.662	148.482	4
	144.129	15.227	117.327	183.753	134.000	140.873	152.880	5
VM	52.345	2.293	49.118	58.800	50.702	51.564	53.771	1
	55.417	2.162	51.682	60.772	54.040	55.005	56.433	2
	57.905	2.527	52.479	63.785	56.038	57.684	59.624	3
	60.688	3.916	54.125	73.422	58.087	59.472	63.835	4
	62.674	3.091	57.217	70.881	60.288	62.238	64.829	5
PEEQ $\times 10^3$	2.905	1.469	0.773	7.032	1.861	2.411	3.819	1
	4.871	1.383	2.486	8.303	3.991	4.606	5.518	2
	6.464	1.625	2.995	10.282	5.266	6.316	7.563	3
	8.280	2.574	4.045	16.846	6.573	7.465	10.315	4
	9.573	2.056	6.018	15.141	7.991	9.252	10.978	5

Table 4
Statistical parameters of von Mises stress (MPa) and equivalent plastic strain components over the matrix of hex-packed RVE when ϵ_{xz} is applied.

	\bar{x}	s	min	max	q ₁	q ₂	q ₃	Voids [%]
VM	74.814	3.430	69.736	89.510	72.745	74.308	76.545	1
	77.689	2.896	73.451	87.416	75.491	77.098	79.608	2
	79.328	4.496	71.179	92.059	76.050	78.479	82.311	3
	80.370	4.091	73.370	91.922	77.422	79.846	82.935	4
	81.582	3.602	74.663	94.649	79.267	81.358	83.314	5
PEEQ $\times 10^3$	17.879	2.465	14.382	28.728	16.376	17.478	19.076	1
	19.932	2.124	16.866	27.139	18.322	19.483	21.329	2
	21.152	3.325	15.338	30.836	18.721	20.498	23.328	3
	21.913	3.038	16.808	30.722	19.721	21.505	23.790	4
	22.806	2.702	17.731	32.946	21.079	22.623	24.072	5

Table 5
Mean values of normal stresses, VM and PEEQ in the random RVE with 4% of voids (MPa).

	$\bar{\sigma}_{xx}^{max}$	$\bar{\sigma}_{yy}^{max}$	$\bar{\sigma}_{zz}^{max}$	VM	PEEQ $\times 10^3$
Fiber	ϵ_{xx}	292.152	214.943	140.808	–
	ϵ_{xz}	60.846	69.204	93.633	–
	ϵ_{yz}	21.111	88.128	40.543	–
Matrix	ϵ_{xx}	374.541	293.848	268.780	122.720
	ϵ_{xz}	152.948	132.924	168.218	139.905
	ϵ_{yz}	52.585	55.886	64.776	165.242

Table 6
Variation of mean normal stress in the random RVE with 4% of void volume fraction compared to minimum and maximum values.

		ϵ_{xx}		ϵ_{xz}	
		% min	% max	% min	% max
Fiber	σ_{xx}^{max}	18.4%	–14.7%	26.2%	–30.0%
	σ_{yy}^{max}	32.0%	–28.5%	45.1%	–47.4%
	σ_{zz}^{max}	10.4%	–19.0%	18.7%	–19.8%
Matrix	σ_{xx}^{max}	11.0%	–22.0%	19.0%	–16.4%
	σ_{yy}^{max}	20.2%	–19.4%	24.5%	–28.7%
	σ_{zz}^{max}	16.0%	–24.6%	17.0%	–23.4%

Table 7
Minimum and maximum values of shear stresses in the random RVE with 4% of void volume fraction (MPa).

		$\bar{\sigma}_{xz}^{max}$		$\bar{\sigma}_{yz}^{max}$		$\bar{\sigma}_{xy}^{max}$	
		min	max	min	max	min	max
Fiber	ϵ_{xx}	35.188	54.992	15.502	33.487	30.185	65.342
	ϵ_{xz}	101.056	110.854	14.159	36.133	15.925	49.321
	ϵ_{yz}	9.041	27.087	90.876	120.552	18.726	29.926
Matrix	ϵ_{xx}	29.597	50.818	17.802	31.130	23.717	38.086
	ϵ_{xz}	74.387	86.757	9.676	23.732	10.639	23.972
	ϵ_{yz}	9.033	21.745	91.202	98.685	31.251	38.442

Table 8

Elastic mechanical properties of constituent materials for the IM7-8552 and the HTA-6376C - elastic and shear moduli in GPa.

Fiber	E_{11}	E_{22}	E_{33}	G_{12}	G_{13}	G_{23}	ν_{12}	ν_{13}	ν_{23}
IM7 (Chamis et al., 2013)	272.50	15.50	15.50	29.00	29.00	7.00	0.20	0.20	0.30
HTA (O'Higgins, 2007)	223.00	23.00	23.00	32.00	32.00	32.00	0.28	0.28	0.28
Matrix	E	ν							
8552 (Chamis et al., 2013)	4.10	0.29							
6376C (O'Higgins, 2007)	3.70	0.20							

matrix. Fig. 29 illustrates the homogenized stress–strain response of the IM7-8552 RVE. The effect of voids on the homogenized response of HTA-6376C is shown in Fig. 30.

The results suggest that:

- Regarding both material systems, the CUF framework shows a good agreement of the homogenized stress–strain curves with experimental benchmarks.
- The presence of voids induces a significant decrease in the homogenized stress.

6. Conclusions

This work has investigated the influence of void volume fraction and RVE thickness on the micromechanical response of composites. A micromechanical framework has been used based on the Carrera Unified Formulation (CUF) and the Component Wise (CW) approach. Three different RVE architectures have been considered: a hex-packed RVE, an RVE with randomly distributed fibers, and a square-packed RVE. Normal and shear strains have been used as loading conditions, and void volume fractions from 1 to 5% and thickness values from 0.1 to 3 mm have been considered. Statistical analyses have been carried out by considering random distributions of voids. The numerical results have shown that:

- Increments of void fractions and thickness lead to higher stress values.
- The choice of the RVE architecture does not affect the maximum stresses significantly.
- The analyses showed the same results when the second RVE was taken into consideration.
- For the considered ranges of void volume fractions, the variation of mean stress values is about 5%–10%.
- For a given void volume fraction, different distributions of voids can lead to differences between maximum stress values of about 30%.
- A slight but considerable difference arises between the macroscopic linear and nonlinear responses. A micromechanical framework involving progressive failures would make nonlinearities more pronounced.
- A significant increase in stress has been observed by changing the RVE thickness from 0.1 to 3 mm.
- Void content has a significant effect on the homogenized stress–strain response of composite, compared to pristine architectures.

Future investigations will incorporate the effect of voids on a multiscale framework, where the constitutive response at a material point interacts with a lower scale through explicit heterogeneous definitions via homogenization, also including the crack nucleation and propagation at the microscale level. Furthermore, the explicit modeling of voids for more detailed localized stress distributions will be considered, and the CUF framework for micromechanical analysis of textile composites will be investigated. Another extension will focus on the thermomechanical analysis and the effects of voids on thermal properties. The effect of voids on the failure onset and its propagation is also under investigation.

Declaration of competing interest

The authors declare that they have no known competing financial interests or personal relationships that could have appeared to influence the work reported in this paper.

Data availability

Data will be made available on request

References

- Aboudi, J., 1981. Generalized effective stiffness theory for the modeling of fiber-reinforced composites. *Int. J. Solids Struct.* 17 (10), 1005–1018.
- Aboudi, J., 1989. Micromechanical Analysis of Composites by the Method of Cells. *Appl. Mech. Rev.* 42 (7), 193–221.
- Aboudi, J., 2004. The Generalized Method of Cells and High-Fidelity Generalized Method of Cells Micromechanical Models — A Review. *Mech. Adv. Mater. Struct.* 11 (4–5), 329–366.
- Aboudi, J., Arnold, S.M., Bednarczyk, B.A., 2012. *Micromechanics of Composite Materials: A Generalized Multiscale Analysis Approach*. Butterworth-Heinemann.
- Aboudi, J., Pindera, M.J., Arnold, S.M., 2001. Linear Thermoelastic Higher-Order Theory for Periodic Multiphase Materials. *J. Appl. Mech.* 68 (5), 697–707.
- Ashouri Vajari, D., González, C., Llorca, J., Legarth, B.N., 2014. A numerical study of the influence of microvoids in the transverse mechanical response of unidirectional composites. *Compos. Sci. Technol.* 97, 46–54.
- Bednarczyk, B.A., Aboudi, J., Arnold, S.M., 2010. Micromechanics Modeling of Composites Subjected to Multiaxial Progressive Damage in the Constituents. *AIAA J.* 48 (7), 1367–1378.
- Blok, L.G., Longana, M.L., Yu, H., Woods, B.K.S., 2018. An investigation into 3D printing of fibre reinforced thermoplastic composites. *Addit. Manuf.* 22, 176–186.
- Carrera, E., Cinefra, M., Petrolo, M., Zappino, E., 2014. Finite Element Analysis of Structures Through Unified Formulation. Wiley, New York.
- Carrera, E., Elishakoff, I., Petrolo, M., 2021. Who needs refined structural theories? *Compos. Struct.* 264, 113671.
- Carrera, E., Kaelel, I., Petrolo, M., 2019. Elastoplastic analysis of compact and thin-walled structures using classical and refined beam finite element models. *Mech. Adv. Mater. Struct.* 26 (3), 274–286.

- Carrera, E., Petrolo, M., 2010. Guidelines and recommendation to construct theories for metallic and composite plates. *AIAA J.* 48 (12), 2852–2866.
- Carrera, E., Petrolo, M., 2012. Refined beam elements with only displacement variables and plate/shell capabilities. *Meccanica* 47 (3), 537–556.
- Carrera, E., Petrolo, M., Nagaraj, M.H., Delicata, M., 2020. Evaluation of the influence of voids on 3D representative volume elements of fiber-reinforced polymer composites using CUF micromechanics. *Compos. Struct.* 254, 112833.
- Chamis, C.C., Abdi, F., Garg, M., Minnetyan, L., Baid, H., Huang, D., Housner, J., Talagani, F., 2013. Micromechanics-based progressive failure analysis prediction for WWFE-III composite coupon test cases. *J. Compos. Mater.* 47 (20–21), 2695–2712.
- Dai, J., Pineda, E.J., Bednarczyk, B.A., Singh, J., Yamamoto, N., 2022. Micromechanics-based simulation of B4C-TiB2 composite fracture under tensile load. *J. Eur. Ceram. Soc.* 42 (14), 6364–6378.
- Dong, J., Huo, N., 2016. A two-scale method for predicting the mechanical properties of 3D braided composites with internal defects. *Compos. Struct.* 152, 1–10.
- Gitman, I.M., 2006. Representative Volumes and Multi-Scale Modelling of Quasi-Brittle Materials (Doctoral Thesis). TU Delft.
- Gitman, I.M., Askes, H., Sluys, L.J., 2007. Representative volume: Existence and size determination. *Eng. Fract. Mech.* 74 (16), 2518–2534.
- Haynes, W., 2013. Probability Distributions. Springer New York, New York, NY, pp. 1752–1754.
- He, Q., Wang, H., Fu, K., Ye, L., 2020. 3D printed continuous CF/PA6 composites: Effect of microscopic voids on mechanical performance. *Compos. Sci. Technol.* 191, 108077.
- Hinton, M., Soden, P.D., Kaddour, A.S., 2004. Failure Criteria in Fibre Reinforced Polymer Composites: The World-Wide Failure Exercise. Elsevier.
- Hsu, D.K., 1988. Ultrasonic Measurements of Porosity in Woven Graphite Polyimide Composites. Springer US, Boston, MA, pp. 1063–1068.
- Huang, Z.M., 2023a. Chapter One - Mechanics Theories for Anisotropic Or Composite Materials. In: *Advances in Applied Mechanics*, vol. 56, Elsevier, pp. 1–137.
- Huang, Z.M., 2023b. True Stress Theory of Matrix in A Composite: A Topical Review. *Materials* 16 (2).
- Huang, T., Gong, Y., 2018. A multiscale analysis for predicting the elastic properties of 3D woven composites containing void defects. *Compos. Struct.* 185, 401–410.
- Jiang, H., Ren, Y., Liu, Z., Zhang, S., 2019. Microscale finite element analysis for predicting effects of air voids on mechanical properties of single fiber bundle in composites. *J. Mater. Sci.* 54 (2), 1363–1381.
- Justo, J., Távora, L., García-Guzmán, L., París, F., 2018. Characterization of 3D printed long fibre reinforced composites. *Compos. Struct.* 185, 537–548.
- Kaleel, I., Petrolo, M., Carrera, E., 2018a. Elastoplastic and progressive failure analysis of fiber-reinforced composites via an efficient nonlinear microscale model. *Aerotec. Missili Spazio* 97, 103–110.
- Kaleel, I., Petrolo, M., Waas, A.M., Carrera, E., 2017. Computationally efficient, high-fidelity micromechanics framework using refined 1D models. *Compos. Struct.* 181, 358–367.
- Kaleel, I., Petrolo, M., Waas, A.M., Carrera, E., 2018b. Micromechanical Progressive Failure Analysis of Fiber-Reinforced Composite Using Refined Beam Models. *J. Appl. Mech. Trans. ASME* 85 (2).
- Khdir, Y.K., Kanit, T., Zairi, F., Nait-Abdelaziz, M., 2014. Computational homogenization of plastic porous media with two populations of voids. *Mater. Sci. Eng. A* 597, 324–330.
- Langford, E., 2006. Quartiles in Elementary Statistics. *J. Stat. Educ.* 14 (3).
- Li, G., Sharifpour, F., Bahmani, A., Montesano, J., 2018. A new approach to rapidly generate random periodic representative volume elements for microstructural assessment of high volume fraction composites. *Mater. Des.* 150, 124–138.
- Li, S., Sitnikova, E., 2019. Representative Volume Elements and Unit Cells: Concepts, Theory, Applications and Implementation. Woodhead Publishing.
- Masmoudi, M., Kaddouri, W., Kanit, T., Madani, S., Ramtani, S., Imad, A., 2017. Modeling of the effect of the void shape on effective ultimate tensile strength of porous materials: Numerical homogenization versus experimental results. *Int. J. Mech. Sci.* 130, 497–507.
- McCarthy, C.T., O'Higgins, R.M., Frizzell, R.M., 2010. A cubic spline implementation of non-linear shear behaviour in three-dimensional progressive damage models for composite laminates. *Compos. Struct.* 92 (1), 173–181.
- Mehdikhani, M., Gorbatikh, L., Verpoest, I., Lomov, S.V., 2019. Voids in fiber-reinforced polymer composites: A review on their formation, characteristics, and effects on mechanical performance. *J. Compos. Mater.* 53 (12), 1579–1669.
- Nagaraj, M.H., Kaleel, I., Carrera, E., Petrolo, M., 2021. Elastoplastic Micromechanical Analysis of Fiber-Reinforced Composites with Defects. *Aerotec. Missili Spazio* 101 (1), 53–59.
- Nemat-Nasser, S., Hori, M., 1999. *Micromechanics: Overall Properties of Heterogeneous Materials*. North-Holland, Amsterdam.
- Neto, E.S., Peric, D., Owen, D., 2008. *Computational Methods for Plasticity Theory and Application*. John Wiley and Sons, Ltd.
- O'Higgins, R.M., 2007. An Experimental and Numerical Study of Damage Initiation and Growth in High Strength Glass and Carbon Fibre-Reinforced Composite Materials (Ph.D. thesis). University of Limerick.
- Pagani, A., Enea, M., Carrera, E., 2022. Quasi-static fracture analysis by coupled three-dimensional peridynamics and high order one-dimensional finite elements based on local elasticity. *Internat. J. Numer. Methods Engrg.* 123 (4), 1098–1113.
- Paley, M., Aboudi, J., 1992. Micromechanical analysis of composites by the generalized cells model. *Mech. Mater.* 14 (2), 127–139.
- Park, S.M., Lim, J.H., Seong, M.R., Sohn, D., 2019. Efficient generator of random fiber distribution with diverse volume fractions by random fiber removal. *Composites B* 167, 302–316.
- Pineda, E.J., 2012. Implementation of a Smeared Crack Band Model in a Micromechanics Framework. NASA technical memorandum, National Aeronautics and Space Administration, Glenn Research Center.
- Pineda, E.J., Bednarczyk, B.A., Ricks, T.M., Farrokh, B., Jackson, W., 2022. Multiscale failure analysis of a 3D woven composite containing manufacturing induced voids and disbonds. *Composites A* 156, 106844.
- Pineda, E.J., Bednarczyk, B.A., Waas, A.M., Arnold, S.M., 2013. Progressive failure of a unidirectional fiber-reinforced composite using the method of cells: Discretization objective computational results. *Int. J. Solids Struct.* 50 (9), 1203–1216.
- Potter, K., Khan, B., Wisnom, M., Bell, T., Stevens, Variability, J., 2008. Fibre waviness and misalignment in the determination of the properties of composite materials and structures. *Composites A* 39 (9), 1343–1354.
- Saenz-Castillo, D., Martín, M.I., Calvo, S., Rodríguez-Lence, F., Güemes, A., 2019. Effect of processing parameters and void content on mechanical properties and NDI of thermoplastic composites. *Composites A* 121, 308–320.
- Stone, D.E.W., Clarke, B., 1975. Ultrasonic attenuation as a measure of void content in carbon-fibre reinforced plastics. *Non-Destructive Testing* 8 (3), 137–145.
- Sun, C.T., Vaidya, R.S., 1996. Prediction of composite properties from a representative volume element. *Compos. Sci. Technol.* 56, 171–179.
- Talreja, R., 2015. Manufacturing defects in composites and their effects on performance. In: Irving, P.E., Soutis, C. (Eds.), *Polymer Composites in the Aerospace Industry*. Woodhead Publishing, pp. 99–113.
- Touliatou, D., Wheel, M.A., 2019. Experimental and numerical analysis of size effects on stress intensity in anisotropic porous materials. *Eng. Fail. Anal.* 104, 772–783.
- Washizu, K., 1968. *Variational Methods in Elasticity and Plasticity*. Pergamon, Oxford.
- Xia, Z., Zhang, Y., Ellyin, F., 2003. A unified periodical boundary conditions for representative volume elements of composites and applications. *Int. J. Solids Struct.* 40 (8), 1907–1921.
- Zhang, Z., Long, Y., Yang, Z., Fu, K., Li, Y., 2022. An investigation into printing pressure of 3D printed continuous carbon fiber reinforced composites. *Composites A* 162, 107162.
- Zhang, Y., Zhou, Z., Zu, S., Tan, Z., 2021. Multiscale numerical investigation on failure behaviour of three-dimensional orthogonal woven carbon/carbon composites subjected to pin-loading. *Ceram. Int.* 47 (22), 31099–31113.